




Article

In-Exchanged CHA Zeolites for Selective Dehydrogenation of Ethane: Characterization and Effect of Zeolite Framework Type

Zen Maeno ^{1,*}, Xiaopeng Wu ¹, Shunsaku Yasumura ¹, Takashi Toyao ^{1,2}, Yasuharu Kanda ³ and Ken-ichi Shimizu ^{1,2,*}

¹ Institute for Catalysis, Hokkaido University, N-21, W-10, Sapporo 001-0021, Japan;

wuxiaopeng@cat.hokudai.ac.jp (X.W.); yasumura@cat.hokudai.ac.jp (S.Y.); toyao@cat.hokudai.ac.jp (T.T.)

² Elements Strategy Initiative for Catalysts and Batteries, Kyoto University, Katsura, Kyoto 615-8520, Japan

³ Applied Chemistry Research Unit, College of Environmental Technology, Graduate School of Engineering, Muroran Institute of Technology, 27-1 Mizumoto, Muroran 050-8585, Japan; kanda@mmm.muroran-it.ac.jp

* Correspondence: maeno@cat.hokudai.ac.jp (Z.M.); kshimizu@cat.hokudai.ac.jp (K.S.)

Received: 3 July 2020; Accepted: 18 July 2020; Published: 20 July 2020



Abstract: In this study, the characterization of In-exchanged CHA zeolite (In-CHA ($\text{SiO}_2/\text{Al}_2\text{O}_3 = 22.3$)) was conducted by in-situ X-ray diffraction (XRD) and ammonia temperature-programmed desorption (NH_3 -TPD). We also prepared other In-exchanged zeolites with different zeolite structures (In-MFI ($\text{SiO}_2/\text{Al}_2\text{O}_3 = 22.3$), In-MOR ($\text{SiO}_2/\text{Al}_2\text{O}_3 = 20$), and In-BEA ($\text{SiO}_2/\text{Al}_2\text{O}_3 = 25$)) and different $\text{SiO}_2/\text{Al}_2\text{O}_3$ ratios (In-CHA(Al-rich) ($\text{SiO}_2/\text{Al}_2\text{O}_3 = 13.7$)). Their catalytic activities in nonoxidative ethane dehydrogenation were compared. Among the tested catalysts, In-CHA(Al-rich) provided the highest conversion. From kinetic experiments and in-situ Fourier transform infrared (FTIR) spectroscopy, $[\text{InH}_2]^+$ ions are formed regardless of $\text{SiO}_2/\text{Al}_2\text{O}_3$ ratio, serving as the active sites.

Keywords: In-exchanged zeolite; reductive solid-state ion-exchange (RSSIE); ethane dehydrogenation; isolated surface hydride

1. Introduction

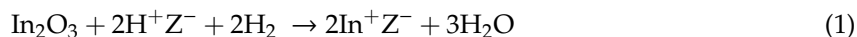
The valorization of ethane is highly demanded in chemical industry owing to increasing availability of inexpensive ethane from shale gas [1,2]. The most frequently used method for this purpose is the steam cracking to obtain ethylene which is an important feedstock for production of various fundamental chemicals, including polyethylene, styrene, ethylene oxide, and acetic acid. However, this method requires high reaction temperature (1073–1173 K) to achieve sufficient ethylene yields [3]. Moreover, the rapid cooling of the outlet gas is necessary for suppression of ethylene polymerization. The steam cracking of ethane is an energy-intensive process. Catalytic dehydrogenation of ethane to ethylene is a promising alternative to decrease the reaction temperature and to conserve energy consumption [4–6]. Various catalyst systems using platinum group metal-based alloys [7–10], Cr [11–13], and Ga [14,15], have been developed. However, the reported systems often suffer from low ethylene selectivity and catalysts deactivation due to coke formation. In addition, the applicability of those processes under industrially meaningful conditions, i.e., high ethane concentration regime, has rarely been investigated [11]. From the practical viewpoint, the development of selective and durable catalyst systems that are workable even under the high concentration conditions is highly demanded.

Zeolites are porous aluminosilicates that comprise tetrahedral SiO_4 and AlO_4 units. To compensate for the cation deficiency derived from the isomorphic substitution of Si^{4+} with Al^{3+} , cationic species such as protons are present on Al sites within pores [16]. These cations are exchangeable with other metal cations through ion-exchange methods. Proton-type and metal-exchanged zeolites show

potential as heterogeneous catalysts for exhaust gas purification and chemical syntheses [17–26]. Numerous different zeolites consisting of 8–12-membered rings with different crystal structures, including CHA (8-membered rings), MFI (10-membered rings), BEA and MOR (12-membered rings), have been developed. The different activities and selectivities of zeolites are closely related to their different pore sizes and crystal structures [27–32]. The SiO₂/Al₂O₃ ratio also affects catalytic properties because the configuration of Al sites and surface properties strongly depend on the ratio [33–37]. Thus, investigating the effects of framework structure and SiO₂/Al₂O₃ ratio in zeolites can help control their catalytic properties, allowing the design of more effective catalysts.

Group 13 metal-exchanged zeolites have attracted much attention as catalysts for the transformation of light alkanes. Ga-exchanged MFI zeolites (Ga-MFI) have been most widely studied since the 1990's [38–41]. Ono and coworkers prepared Ga-MFI using liquid-phase ion-exchange and then investigated the mechanism of the dehydrocyclodimerization (DHCD) of propane to aromatics [42]. Improving the activity of Ga-MFI by loading larger amounts of Ga species through reductive solid-state ion-exchange (RSSIE) was investigated [43]. Several cationic Ga species, such as Ga⁺, [GaH]²⁺, and [GaH₂]⁺ ions, have been reported as catalytically active species for the dehydrogenation of propane [44–46]. Recently, Bell and coworkers reported that [GaH]²⁺ rather than [GaH₂]⁺ ions are active species using a combination of kinetic, spectroscopic, and theoretical studies [47], whereas Lewis–Brønsted acid pairs (Ga⁺ and H⁺) have been proposed as active sites by the group of Lercher based on their investigation of the Ga/Al effect and acidity characterization along with theoretical investigation [48]. Various Ga-exchanged zeolites including Ga-MFI have been applied to the transformation of other light alkanes to aromatic compounds, the dehydrogenation of light alkanes, and reactions of methane with light alkenes to produce higher hydrocarbons [49–51].

In contrast to that by Ga-exchanged zeolites, studies on dehydrogenative transformation of light alkanes by In-exchanged zeolites have been rarely reported. Their preparation by RSSIE between In₂O₃ and proton-type zeolites has been studied by several groups [52]. The reaction is described in Equation (1).



where Z[−] denotes a zeolite anion. In the context of catalysis, Hert and coworkers prepared In-exchanged MFI (In-MFI) by RSSIE and compared its catalytic activity for propane DHCD with that of Ga-MFI [53,54]. They reported that In-MFI exhibits poor durability due to the reduction of active In⁺ cations to In metal during the reaction. The reaction of methane with ethylene/benzene was investigated by the group of Baba using In-MFI, for which the activation of methane at In⁺ cations coordinated to zeolite anions was proposed [55]. Recently, our research group has reported that In-exchanged CHA zeolite (In-CHA) catalyzes the selective dehydrogenation of ethane and exhibits high durability [56]. A combination of experimental and theoretical studies revealed that [InH₂]⁺ ions, which are formed in situ through the reaction of In⁺ cations with H₂, serve as catalytically active sites. However, the detailed investigation including effects of zeolite framework and SiO₂/Al₂O₃ on ethane dehydrogenation were not conducted.

As a continuation of our previous study, we herein report the detailed characterization of In-CHA by in-situ X-ray diffraction (XRD) and ammonia temperature-programmed desorption (NH₃-TPD). We also investigated the effect of zeolite framework and SiO₂/Al₂O₃ to achieve higher conversion compared to In-CHA. In-MFI, In-MOR, and In-BEA exhibit inferior activities compared to that of In-CHA, whereas a higher conversion value was achieved using In-CHA with a higher Al content (In-CHA(Al-rich)). Kinetic study and in-situ Fourier transform infrared (FTIR) spectroscopy indicated that [InH₂]⁺ ions are formed in CHA zeolites regardless of SiO₂/Al₂O₃ ratio, and that they serve as catalytically active sites for the dehydrogenation of ethane.

2. Results

2.1. XRD

The RSSIE reactions of In_2O_3 and zeolites under H_2 at high temperature have been investigated by H_2 temperature-programmed reduction (H_2 -TPR) and/or thermogravimetric analysis in several previous studies [52,54,57]. However, in-situ characterization of In_2O_3 and zeolites has not been reported yet. We have reported the preparation of In-CHA through RSSIE of CHA-supported In_2O_3 obtained by impregnation ($\text{In}_2\text{O}_3/\text{CHA}$), revealing the formation of highly dispersed In species by spectroscopic and microscopic analysis [58]. In this study, in-situ XRD was conducted for RSSIE of $\text{In}_2\text{O}_3/\text{CHA}$ under 5% H_2/N_2 flow. Figure 1a shows a series of XRD patterns obtained at different temperatures. The characteristic peak at $2\theta = 30.6^\circ$ derived from In_2O_3 (222) [59] and the typical diffraction pattern of CHA zeolites [60] were observed at 303 and 473 K, respectively. The intensity of the peak derived from In_2O_3 was slightly decreased at 573 K and the peak was no longer observed at 773 K (Figure 1b). After cooling to 303 K, no peaks derived from In_2O_3 were observed. The sharp peaks in the zeolite diffraction patterns at $2\theta = 9.6^\circ$ and 20.8° decreased in intensity above 573 K due to temperature-induced disordering and then returned to their initial intensities upon cooling from 773 to 303 K [61]. These observations indicate the occurrence of RSSIE reaction at temperatures from 573 to 773 K, which is consistent with the results of H_2 -TPR measurement in our previous study [56]. A series of In-exchanged zeolites including In-MFI, In-MOR, In-BEA, and In-CHA(Al-rich) were also prepared through similar RSSIE reactions of In_2O_3 supported on the corresponding zeolites. The XRD measurements showed that the peaks assignable to In_2O_3 (222), (400), and (440) disappeared after RSSIE in each case (Figure 2), indicating the high dispersion of In species.

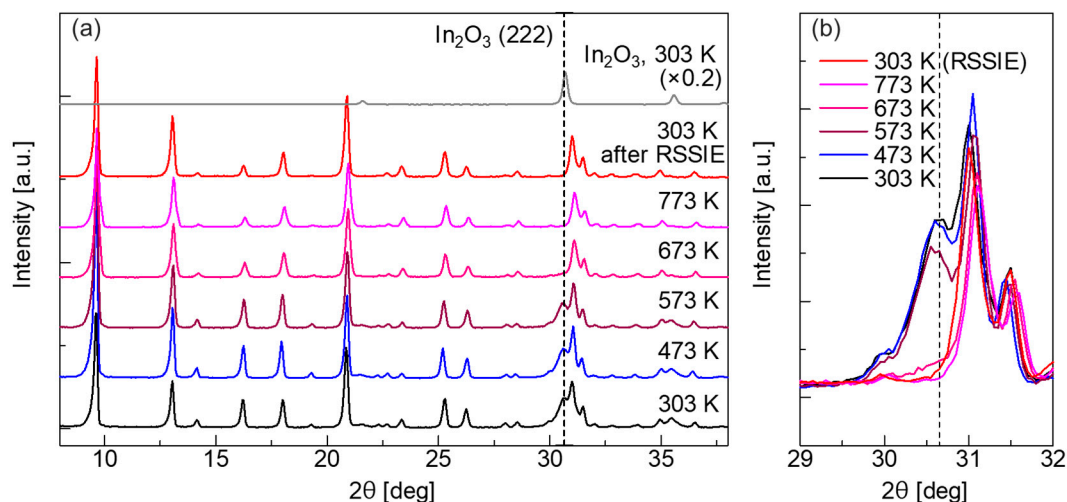


Figure 1. (a) In-situ X-ray diffraction (XRD) patterns during reductive solid-state ion-exchange (RSSIE) of $\text{In}_2\text{O}_3/\text{CHA}$ ($\text{In}/\text{Al} = 0.8$) under 5% H_2/N_2 flow at different temperatures. (b) Comparison of the peaks derived from In_2O_3 (222) around $2\theta = 30.6^\circ$.

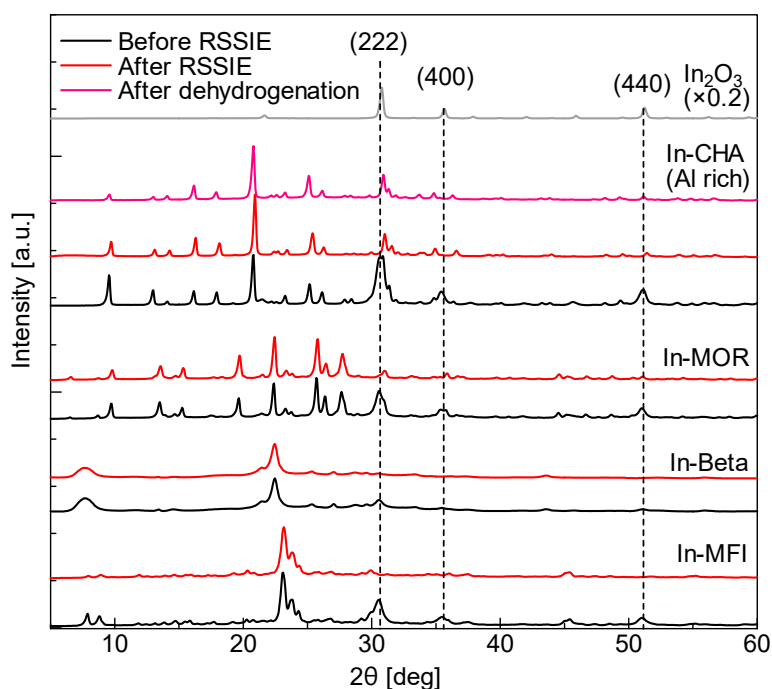


Figure 2. XRD patterns for In-MFI, In-BEA, In-MOR, and In-CHA(Al-rich) before (black) and after (red) RSSIE and for In-CHA(Al-rich) after the ethane dehydrogenation at 993 K (pink). The patterns were obtained at room temperature.

2.2. NH_3 -TPD

The acidity profiles of In-CHA samples with different In/Al values (In/Al = 0.2, 0.4, and 0.8) were investigated by NH_3 -TPD. In each case, the catalyst was exposed to NH_3/He at 473 K followed by purging with He. Thereafter, the temperature was increased from 473 to 973 K under He flow while the desorbed NH_3 ($m/z = 16$) was monitored. The TPD profiles of proton-type CHA (H-CHA) and a series of In-CHA samples are shown in Figure 3. The profile of H-CHA showed a wide peak around 700–800 K due to NH_3 desorbed from Brønsted acid sites. The intensity of the peak decreased with the increase of In/Al. This trend is similar to that observed in the NH_3 adsorption experiment [56]. In addition, a desorption peak around 600 K appeared upon In loading and its intensity increased with In/Al ratio. This peak might be due to NH_3 weakly adsorbed on In^+ cations [62]. The results of NH_3 -TPD are consistent with the occurrence of RSSIE reactions as described in Equation (1).

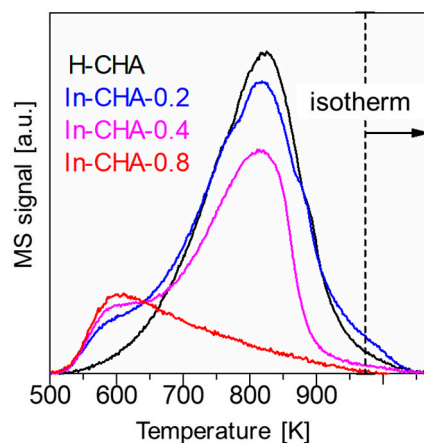


Figure 3. Ammonia temperature-programmed desorption (NH_3 -TPD) profiles for H-CHA and different In-CHA samples.

2.3. Effect of Zeolite Host upon Ethane Dehydrogenation Catalyzed by In-Exchanged Zeolites

We previously found that In-CHA with $\text{SiO}_2/\text{Al}_2\text{O}_3 = 22.3$ and $\text{In}/\text{Al} = 0.8$ exhibits high selectivity for dehydrogenation of ethane to ethylene and carbon balance at 933 K. In this work, In-MFI, In-MOR, and In-BEA having similar $\text{SiO}_2/\text{Al}_2\text{O}_3$ ratios (22.3, 20.0, and 25.0, respectively) and In-CHA(Al-rich) ($\text{SiO}_2/\text{Al}_2\text{O}_3 = 13.7$) were prepared using the same In/Al value of 0.8 and compared with In-CHA in ethane dehydrogenation (Table 1). In-MFI, In-MOR, and In-BEA showed lower conversions of 12.9%, 14.9%, and 13.5%, respectively, than that for In-CHA (25.9%) (entries 1–3 vs. entry 5) despite their larger zeolite pores ($5.6 \text{ \AA} \times 5.3 \text{ \AA}$, $7.0 \text{ \AA} \times 6.5 \text{ \AA}$, and $7.6 \text{ \AA} \times 7.3 \text{ \AA}$, respectively) compared to that of CHA ($3.8 \text{ \AA} \times 3.6 \text{ \AA}$). In contrast, In-CHA(Al-rich) exhibited a superior conversion (37.9%) while maintaining the high selectivity of 96.1% (entry 5). For all the In-exchanged zeolites, high selectivity for ethylene (>96%) and carbon balance (>93%) were observed while main byproduct was methane.

Table 1. Conversion, selectivity, and carbon balance values for 30 min of ethane dehydrogenation at 933 K using several In-exchanged zeolites.

$$\begin{array}{c} \text{H} & & \text{H} \\ & \backslash & / \\ & \text{C} - & \text{C} - \text{H} \\ & / & \backslash \\ \text{H} & & \text{H} \end{array} \xrightarrow[933 \text{ K, } -\text{H}_2]{\text{In-zeolite catalyst (0.1 g)}} \begin{array}{c} \text{H} & & \text{H} \\ & \backslash & / \\ & \text{C} = & \text{C} \\ & / & \backslash \\ \text{H} & & \text{H} \end{array} + \text{CH}_4 + \text{Coke}$$

Entry	Catalyst	$\text{SiO}_2/\text{Al}_2\text{O}_3$	In/Al	Conv. [%] ^a	Sel. [%] ^a	Carbon Balance [%] ^a
1	In-MFI	22.3	0.8	12.9	99.2	99
2	In-MOR	20.0	0.8	14.9	97.6	99
3	In-BEA	25.0	0.8	13.5	97.5	94
4	In-CHA(Al-rich)	13.7	0.8	37.9	96.6	98
5	In-CHA ^b	22.3	0.8	25.9	96.1	99

Reaction conditions: 0.1 g of catalyst, 10% $\text{C}_2\text{H}_6/\text{He}$ (10 mL/min). [^a] The determination was performed using a gas chromatography (GC). [^b] The data were previously reported in our paper [56].

The ethane dehydrogenation was conducted under severe reaction condition (80% $\text{C}_2\text{H}_6/\text{N}_2$, 993 K) using 0.1 g of In-CHA(Al-rich) (Figure 4). The conversion and selectivity values at 1 h were 32.7% and 90.7%, respectively. Although the conversion value decreased to 30.9% during the 40 h reaction, good selectivity was maintained. This catalytic performance is comparable with those of other reported catalyst systems for nonoxidative ethane dehydrogenation [4]. The catalyst was reusable after regeneration treatment (50% O_2/N_2 for 60 min and 10% H_2/N_2 for 30 min at 993 K) without significant loss of activity or selectivity (32.5% conversion and 90.8% selectivity at 1 h) (Figure 4). The diffraction pattern derived from CHA framework was maintained after the reaction, as confirmed by XRD measurement (Figure 2), which is consistent with the high reusability of In-CHA(Al-rich).

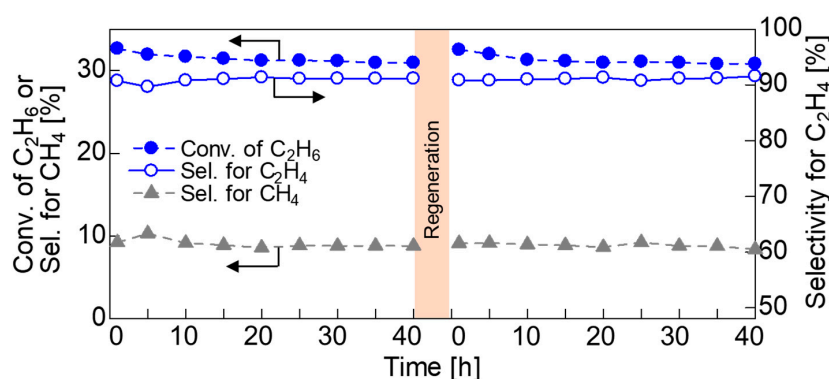


Figure 4. Time course of ethane dehydrogenation using In-CHA(Al-rich) under a high concentration of ethane at 993 K.

Previously, we investigated the active species ($[\text{InH}_2]^+$, $[\text{InH}]^{2+}$, or In^+ cations) for ethane dehydrogenation catalyzed by In-CHA based on kinetic and in-situ spectroscopic studies with transition state (TS) calculations [56]. The TS calculations revealed that the calculated activation enthalpies (ΔH^\ddagger) for C–H activation of ethane on In hydrides ($[\text{InH}_2]^+$ or $[\text{InH}]^{2+}$ ions) are ca. 200–240 kJ/mol, whereas that on In^+ cations is much higher (ca. 400 kJ/mol). The experimental ΔH^\ddagger value for ethane dehydrogenation based on Eyring plot was determined as 236 kJ/mol, suggesting that the catalytically active sites are In hydrides. To obtain insight into the effect of the zeolite, the turnover frequency (TOF) values normalized to the total amount of In species were compared (Figure 5a). The TOF value for In-CHA(Al-rich) was similar to that for In-CHA and was more than five-time higher than those for other In-zeolites. Eyring plots for ethane dehydrogenation were also investigated. The obtained plots are shown in Figure 5b with estimated apparent ΔH^\ddagger values. The ΔH^\ddagger of In-CHA(Al-rich) was determined to be 258 kJ/mol, which is similar to that for In-CHA, while In-MFI, In-MOR, and In-BEA showed much higher ΔH^\ddagger values (364, 300, and 322 kJ/mol, respectively). Comparison of TOF and ΔH^\ddagger values among In-zeolites indicates that (1) In hydrides ($[\text{InH}_2]^+$ or $[\text{InH}]^{2+}$ ions) are possible active sites for In-CHA(Al-rich) rather than In^+ cations and that (2) the active species and/or reaction mechanism are different between In-CHA zeolites and other In-exchanged zeolites.

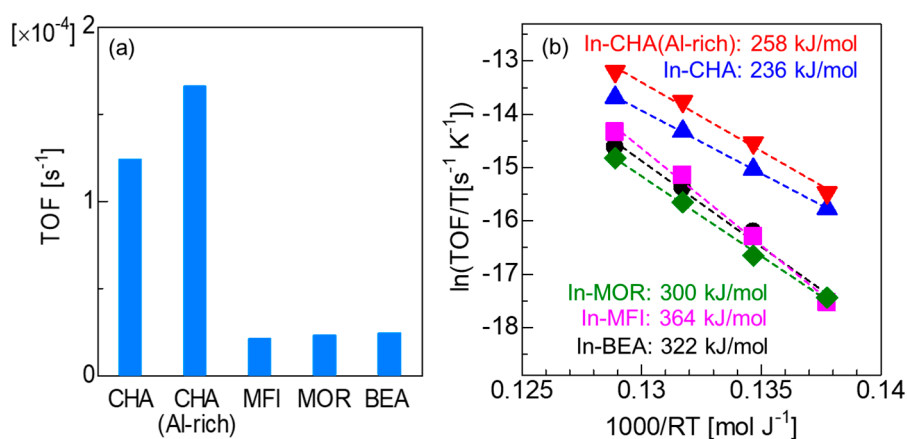


Figure 5. (a) Effect of zeolite host on turnover frequency (TOF) normalized to amount of In obtained at 873 K. (b) Eyring plots and apparent activation enthalpies for the ethane dehydrogenation (873–933 K) using In-MFI (pink), In-MOR (green), In-BEA (black), and In-CHA(Al-rich) (red). The plots were obtained under conditions obtaining ethane conversions below 15%. The data for In-CHA (blue) were previously reported in our previous paper [56].

Furthermore, in-situ FTIR spectroscopy was conducted for In-CHA(Al-rich) to determine possible In hydrides in In-CHA(Al-rich). After H_2 treatment at 773 K, the band derived from the stretching vibration of In–H ($\nu(\text{In–H})$) appeared around 1700 cm^{-1} (Figure 6a). This band can be deconvoluted into two peaks assignable to $\nu(\text{In–H})$ (1777 and 1715 cm^{-1}) with other peaks (1661 and 1610 cm^{-1}) (Figure 6b). Based on our previous vibration analysis by density functional theory calculations [56], the highest peak at 1715 cm^{-1} is derived from the symmetric $\nu(\text{In–H})$ of $[\text{InH}_2]^+$ ions, while the smaller peak at 1777 cm^{-1} is assignable to the asymmetric $\nu(\text{In–H})$ of $[\text{InH}_2]^+$ ions or the $\nu(\text{In–H})$ of $[\text{InH}]^{2+}$ ions. These results indicate that the main In hydrides are $[\text{InH}_2]^+$ rather than $[\text{InH}]^{2+}$ in In-CHA(Al-rich). The other peaks might be derived from different-type adsorbed water molecules [63,64]. From the above combined results, $[\text{InH}_2]^+$ ions are likely formed in In-CHA zeolites regardless of $\text{SiO}_2/\text{Al}_2\text{O}_3$ ratio and are likely to be the active sites.

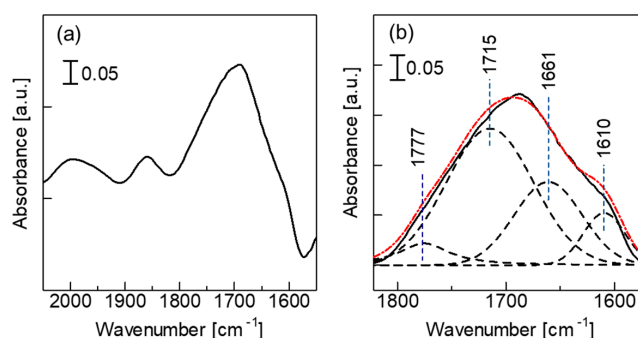


Figure 6. (a) In-situ Fourier transform infrared (FTIR) spectra for In-CHA(Al-rich) measured at 153 K after H₂ treatment at 773 K. (b) Deconvolution of the band around 1700 cm⁻¹.

3. Materials and Methods

3.1. Catalyst Preparation

The preparation of In-CHA was conducted according to our previous study [58]. In₂O₃ immobilized on CHA zeolite (In₂O₃/CHA) was obtained from In(NO₃)₃·nH₂O (purchased from Kanto Chemical Co., Inc., Japan) and the NH₄⁺-type CHA zeolite (Tosoh, SiO₂/Al₂O₃ = 22.3) through impregnation and calcination under air. Next, the RSSIE of In₂O₃/CHA was carried out under H₂ flow at 773 K to obtain In-CHA. Other In-exchanged zeolites (In-MFI, In-MOR, In-BEA, and In-CHA(Al-rich)) were obtained in a similar manner from MFI (Tosoh, SiO₂/Al₂O₃ = 22.3, HSZ-820NHA), MOR (Tosoh, SiO₂/Al₂O₃ = 20, JRC-Z-HM20), BEA (SiO₂/Al₂O₃ = 25, JRC-Z-HB25, provided by the Catalysis Society of Japan, Japan), and CHA (Tosoh, SiO₂/Al₂O₃ = 13.7). The In/Al ratio was estimated from the amounts of In(NO₃)₃·nH₂O. H-CHA was prepared by calcination of NH₄⁺-type CHA at 873 K under air for 1 h.

3.2. XRD

In-situ XRD measurements during RSSIE of In₂O₃/CHA was conducted using a Cu Kα radiation source (Rigaku Ultima IV, Rigaku Corporation, Japan). XRD patterns were obtained while heating In₂O₃/CHA from 303 to 773 K at 20 K/min under 5% H₂/N₂ flow (100 mL/min). For ex-situ XRD measurements, a Rigaku MiniFlex II/AP diffractometer with Cu Kα radiation (Rigaku Corporation, Japan) was used.

3.3. NH₃-TPD

NH₃-TPD experiments were investigated using a BELCAT (MicrotracBEL, Japan). The In-CHA with different In/Al ratio (0.2, 0.4, and 0.8) was prepared in situ under 5% H₂/Ar at 773 K and then treated with 10% NH₃/He at 473 K followed by He purge. After these treatments, the sample was heated from 473 to 973 K under He flow while the desorbed NH₃ (*m/z* = 16) was monitored by a mass spectrometer (BELMass (MicrotracBEL, Japan)).

3.4. Catalytic Tests

Non-oxidative dehydrogenation of ethane was performed in a fixed-bed continuous flow system at 933 K. The catalyst was prepared in situ by treatment of a 0.1 g of the In₂O₃ immobilized on the corresponding zeolite under 10% H₂/He flow (50 mL/min) at 773 K followed by He purge before the reaction. Thereafter, the catalyst was heated to 933 K, and 10% C₂H₆/He (10 mL/min) was introduced. For determination of conversions, yields, and selectivities, gas chromatography (GC) analysis was conducted using Shimadzu GC-14B (Shimadzu Corporation, Japan) combined with a SHINCARBON ST or a Unipack S column (Shinwa Chemical Industry Ltd., Japan). For dehydrogenation under a high

concentration of ethane, the in-situ preparation of In-CHA(Al-rich) was carried out under 80% H₂/N₂ (10 mL/min) at 993 K for 30 min, and the reaction was investigated at the same temperature under 10 mL/min of 80% C₂H₆/N₂. The GC analysis was performed using an Agilent 490 micro-GC with a thermal conductivity detector. The conversion, selectivity, carbon balance, and TOF were calculated as follows.

$$\text{Conv. [\%]} = \frac{[\text{ethane}]_{\text{init}} - [\text{ethane}]}{[\text{ethane}]_{\text{init}}} \times 100$$

$$\text{Selec. [\%]} = \frac{[\text{ethylene}]}{[\text{ethylene}] + [\text{methane}]} \times 100$$

$$\text{Carbon balance [\%]} = \frac{([\text{ethane}] + [\text{ethylene}] + [\text{methane}])}{[\text{ethane}]_{\text{init}}} \times 100$$

$$\text{TOF [s}^{-1}\text{]} = \frac{\text{Formation rate of ethane [mmol}\cdot\text{s}^{-1}\text{]}}{\text{Total In amount [mmol]}}$$

3.5. In-Situ FTIR Spectroscopy

FTIR spectroscopy study was conducted using a home-made in-situ cell and FT/IR-4100 (JASCO, Japan) with a mercury cadmium telluride detector. Prior to measurement, In-CHA was prepared in situ by H₂ treatment of a self-supported disk of In₂O₃/CHA (ca. 40 mg) at 773 K and was then kept under vacuum at 773 K for 2 h. After taking a background spectrum below 153 K cooling the cell using liquid N₂, the sample was treated with H₂ flow at 773 K for 2 h. Then, the temperature was decreased to below 153 K again and the FTIR spectra were recorded without exposure to air.

4. Conclusions

In this work, a detailed characterization of In-CHA and the effect of zeolite on ethane dehydrogenation were described. In-situ XRD revealed that the RSSIE of In₂O₃/CHA occurs without decomposition of the zeolite framework. NH₃-TPD measurement showed that the amount of acid sites decreases with the increase of In loading amount. In the catalytic dehydrogenation of ethane, In-CHA(Al-rich) exhibits the highest conversion value among the In-exchanged zeolites, including In-MFI, In-MOR, and In-BEA. The combined results of kinetic experiments and in-situ FTIR spectroscopy suggest that [InH₂]⁺ ions are plausible active In-hydrides for In-CHA(Al-rich) and that the active In species and/or reaction mechanism for other In-exchanged zeolites are different from those of In-CHA. This study indicates that the small pores in CHA zeolites play an important role in their unique catalytic activity. We are now investigating the effect of CHA pores on the formation of In hydrides and the reaction mechanism of ethane dehydrogenation.

Author Contributions: Z.M. designed the experiments and wrote the draft; X.W. examined the catalyst preparations and ethane dehydrogenations; S.Y. conducted NH₃-TPD and in-situ FTIR spectroscopy; T.T. and K.S. critically revised the manuscript. Y.K. conducted in-situ XRD measurements and analyzed the data. All authors have read and agreed to the published version of the manuscript.

Funding: This work was financially supported by a JSPS KAKENHI (No. 17H01341, 20H02518, and 20H02775) from the Japan Society for the Promotion of Science (JSPS) as well as by the Japanese Ministry of Education, Culture, Sports, Science, and Technology (MEXT) within the projects “Elements Strategy Initiative to Form Core Research Center” (JPMXP0112101003). This was also supported by the JST-CREST projects JPMJCR17J3 and JPMJCR15P4.

Acknowledgments: The authors would like to thank the staffs in technical division of the Institute for Catalysis (Hokkaido University) for experimental setup.

Conflicts of Interest: The authors declare no conflict of interest.

References

1. Boulamanti, A.; Moya, J.A. Production Costs of the Chemical Industry in the EU and Other Countries: Ammonia, Methanol and Light Olefins. *Renew. Sustain. Energy Rev.* **2017**, *68*, 1205–1212. [[CrossRef](#)]

2. Siirola, J.J. The Impact of Shale Gas in the Chemical Industry. *AIChE J.* **2014**, *7*, 810–819. [[CrossRef](#)]
3. Grace Chan, K.Y.; Inal, F.; Senkan, S. Suppression of Coke Formation in the Steam Cracking of Alkanes: Ethane and Propane. *Ind. Eng. Chem. Res.* **2002**, *37*, 901–907. [[CrossRef](#)]
4. Saito, H.; Sekine, Y. Catalytic Conversion of Ethane to Valuable Products through Non-Oxidative Dehydrogenation and Dehydroaromatization. *RSC Adv.* **2020**, *10*, 21427–21453. [[CrossRef](#)]
5. James, O.O.; Mandal, S.; Alele, N.; Chowdhury, B.; Maity, S. Lower Alkanes Dehydrogenation: Strategies and Reaction Routes to Corresponding Alkenes. *Fuel Process. Technol.* **2016**, *149*, 239–255. [[CrossRef](#)]
6. Sattler, J.J.H.B.; Ruiz-Martinez, J.; Santillan-Jimenez, E.; Weckhuysen, B.M. Catalytic Dehydrogenation of Light Alkanes on Metals and Metal Oxides. *Chem. Rev.* **2014**, *114*, 10613–10653. [[CrossRef](#)]
7. Galvita, V.; Siddiqi, G.; Sun, P.; Bell, A.T. Ethane Dehydrogenation on Pt/Mg(Al)O and PtSn/Mg(Al)O Catalysts. *J. Catal.* **2010**, *271*, 209–219. [[CrossRef](#)]
8. Wegener, E.C.; Wu, Z.; Tseng, H.T.; Gallagher, J.R.; Ren, Y.; Diaz, R.E.; Ribeiro, F.H.; Miller, J.T. Structure and Reactivity of Pt–In Intermetallic Alloy Nanoparticles: Highly Selective Catalysts for Ethane Dehydrogenation. *Catal. Today* **2018**, *299*, 146–153. [[CrossRef](#)]
9. Fang, S.; Zhang, K.; Wang, C.; Ma, L.; Zhang, Q.; Liu, Q.; Chen, L.; Chen, L.; Zhang, Q.; Tian, Z. The Properties and Catalytic Performance of PtSn/Mg(x-Ga)AlO Catalysts for Ethane Dehydrogenation. *RSC Adv.* **2017**, *7*, 22836–22844. [[CrossRef](#)]
10. Wu, Z.; Wegener, E.C.; Tseng, H.T.; Gallagher, J.R.; Harris, J.W.; Diaz, R.E.; Ren, Y.; Ribeiro, F.H.; Miller, J.T. Pd–In Intermetallic Alloy Nanoparticles: Highly Selective Ethane Dehydrogenation Catalysts. *Catal. Sci. Technol.* **2016**, *6*, 6965–6976. [[CrossRef](#)]
11. Shi, X.; Ji, S.; Li, C. Oxidative Dehydrogenation of Ethane with CO₂ over Novel Cr/SBA-15/Al₂O₃/FeCrAl Monolithic Catalysts. *Energy Fuels* **2008**, *22*, 3631–3638. [[CrossRef](#)]
12. Nakagawa, K.; Kajita, C.; Ikenaga, N.O.; Suzuki, T.; Kobayashi, T.; Nishitani-Gamo, M.; Ando, T. The Role of Chemisorbed Oxygen on Diamond Surfaces for the Dehydrogenation of Ethane in the Presence of Carbon Dioxide. *J. Phys. Chem. B* **2003**, *107*, 4048–4056. [[CrossRef](#)]
13. Zhao, X.; Wang, X. Oxidative Dehydrogenation of Ethane to Ethylene by Carbon Dioxide over Cr/TS-1 Catalysts. *Catal. Commun.* **2006**, *7*, 633–638. [[CrossRef](#)]
14. Nakagawa, K.; Okamura, M.; Ikenaga, N.; Suzuki, T.; Kobayashi, T. Dehydrogenation of Ethane over Gallium Oxide in the Presence of Carbon Dioxide. *Chem. Commun.* **1998**, *3*, 1025–1026. [[CrossRef](#)]
15. Lei, T.; Cheng, Y.; Miao, C.; Hua, W.; Yue, Y.; Gao, Z. Silica-Doped TiO₂ as Support of Gallium Oxide for Dehydrogenation of Ethane with CO₂. *Fuel Process. Technol.* **2018**, *177*, 246–254. [[CrossRef](#)]
16. Cejka, J.; Corma, A.; Zones, S. (Eds.) *Zeolites and Catalysis: Synthesis, Reactions and Applications*; Wiley-VCH Verlag GmbH & Co. KGaA: Weinheim, Germany, 2010.
17. Marberger, A.; Petrov, A.W.; Steiger, P.; Elsener, M.; Kröcher, O.; Nachttegaal, M.; Ferri, D. Time-Resolved Copper Speciation during Selective Catalytic Reduction of NO on Cu-SSZ-13. *Nat. Catal.* **2018**, *1*, 221–227. [[CrossRef](#)]
18. Moliner, M.; Corma, A. From Metal-Supported Oxides to Well-Defined Metal Site Zeolites: The next Generation of Passive NO_x Adsorbers for Low-Temperature Control of Emissions from Diesel Engines. *React. Chem. Eng.* **2019**, *4*, 223–234. [[CrossRef](#)]
19. Song, J.; Wang, Y.; Walter, E.D.; Washton, N.M.; Mei, D.; Kovarik, L.; Engelhard, M.H.; Proding, S.; Wang, Y.; Peden, C.H.F.; et al. Toward Rational Design of Cu/SSZ-13 Selective Catalytic Reduction Catalysts: Implications from Atomic-Level Understanding of Hydrothermal Stability. *ACS Catal.* **2017**, *7*, 8214–8227. [[CrossRef](#)]
20. Battiston, A.A.; Bitter, J.H.; Koningsberger, D.C. Reactivity of Binuclear Fe Complexes in Over-Exchanged Fe/ZSM5, Studied by in Situ XAFS Spectroscopy 2. Selective Catalytic Reduction of NO with Isobutane. *J. Catal.* **2003**, *218*, 163–177. [[CrossRef](#)]
21. Kosinov, N.; Liu, C.; Hensen, E.J.M.; Pidko, E.A. Engineering of Transition Metal Catalysts Confined in Zeolites. *Chem. Mater.* **2018**, *30*, 3177–3198. [[CrossRef](#)] [[PubMed](#)]
22. Luo, W.; Cao, W.; Bruijninx, P.C.A.; Lin, L.; Wang, A.; Zhang, T. Zeolite-Supported Metal Catalysts for Selective Hydrodeoxygenation of Biomass-Derived Platform Molecules. *Green Chem.* **2019**, *21*, 3744–3768. [[CrossRef](#)]
23. Harris, J.W.; Liao, W.C.; Di Iorio, J.R.; Henry, A.M.; Ong, T.C.; Comas-Vives, A.; Copéret, C.; Gounder, R. Molecular Structure and Confining Environment of Sn Sites in Single-Site Chabazite Zeolites. *Chem. Mater.* **2017**, *29*, 8824–8837. [[CrossRef](#)]

24. Ichihashi, H.; Sato, H. The Development of New Heterogeneous Catalytic Processes for the Production of ϵ -Caprolactam. *Appl. Catal. A Gen.* **2001**, *221*, 359–366. [\[CrossRef\]](#)
25. Nakamura, K.; Okuda, A.; Ohta, K.; Matsubara, H.; Okumura, K.; Yamamoto, K.; Itagaki, R.; Suganuma, S.; Tsuji, E.; Katada, N. Direct Methylation of Benzene with Methane Catalyzed by Co/MFI Zeolite. *ChemCatChem* **2018**, *10*, 3806–3812. [\[CrossRef\]](#)
26. Tomkins, P.; Ranocchiari, M.; van Bokhoven, J.A. Direct Conversion of Methane to Methanol under Mild Conditions over Cu-Zeolites and Beyond. *Acc. Chem. Res.* **2017**, *50*, 418–425. [\[CrossRef\]](#)
27. Shi, J.; Wang, Y.; Yang, W.; Tang, Y.; Xie, Z. Recent Advances of Pore System Construction in Zeolite-Catalyzed Chemical Industry Processes. *Chem. Soc. Rev.* **2015**, *44*, 8877–8903. [\[CrossRef\]](#)
28. Dusselier, M.; Davis, M.E. Small-Pore Zeolites: Synthesis and Catalysis. *Chem. Rev.* **2018**, *118*, 5265–5329. [\[CrossRef\]](#)
29. Deka, U.; Lezcano-Gonzalez, I.; Weckhuysen, B.M.; Beale, A.M. Local Environment and Nature of Cu Active Sites in Zeolite-Based Catalysts for the Selective Catalytic Reduction of NO_x. *ACS Catal.* **2013**, *3*, 413–427. [\[CrossRef\]](#)
30. Gounder, R.; Iglesia, E. The Roles of Entropy and Enthalpy in Stabilizing Ion-Pairs at Transition States in Zeolite Acid Catalysis. *Acc. Chem. Res.* **2012**, *45*, 229–238. [\[CrossRef\]](#)
31. Mahyuddin, M.H.; Staykov, A.; Shiota, Y.; Miyanishi, M.; Yoshizawa, K. Roles of Zeolite Confinement and Cu-O-Cu Angle on the Direct Conversion of Methane to Methanol by [Cu₂(μ -O)]²⁺-Exchanged AEI, CHA, AFX, and MFI Zeolites. *ACS Catal.* **2017**, *7*, 3741–3751. [\[CrossRef\]](#)
32. Lusardi, M.; Chen, T.T.; Kale, M.; Kang, J.H.; Neurock, M.; Davis, M.E. Carbonylation of Dimethyl Ether to Methyl Acetate over SSZ-13. *ACS Catal.* **2020**, *10*, 842–851. [\[CrossRef\]](#)
33. Otomo, R.; Yokoi, T.; Tatsumi, T. Synthesis of Isosorbide from Sorbitol in Water over High-Silica Aluminosilicate Zeolites. *Appl. Catal. A Gen.* **2015**, *505*, 28–35. [\[CrossRef\]](#)
34. Goto, D.; Harada, Y.; Furumoto, Y.; Takahashi, A.; Fujitani, T.; Oumi, Y.; Sadakane, M.; Sano, T. Conversion of Ethanol to Propylene over HZSM-5 Type Zeolites Containing Alkaline Earth Metals. *Appl. Catal. A Gen.* **2010**, *383*, 89–95. [\[CrossRef\]](#)
35. Arudra, P.; Bhuiyan, T.I.; Akhtar, M.N.; Aitani, A.M.; Al-Khattaf, S.S.; Hattori, H. Silicalite-1 as Efficient Catalyst for Production of Propene from 1-Butene. *ACS Catal.* **2014**, *4*, 4205–4214. [\[CrossRef\]](#)
36. Zhao, L.; Gao, J.; Xu, C.; Shen, B. Alkali-Treatment of ZSM-5 Zeolites with Different SiO₂/Al₂O₃ Ratios and Light Olefin Production by Heavy Oil Cracking. *Fuel Process. Technol.* **2011**, *92*, 414–420. [\[CrossRef\]](#)
37. Wan, Z.; Wu, W.; Li, G.K.; Wang, C.; Yang, H.; Zhang, D. Effect of SiO₂/Al₂O₃ Ratio on the Performance of Nanocrystal ZSM-5 Zeolite Catalysts in Methanol to Gasoline Conversion. *Appl. Catal. A Gen.* **2016**, *523*, 312–320. [\[CrossRef\]](#)
38. Chen, N.Y.; Yan, T.Y. M2 Forming a Process for Aromatization of Light Hydrocarbons. *Ind. Eng. Chem. Process Des. Dev.* **1986**, *25*, 151–155. [\[CrossRef\]](#)
39. Seddon, D. Paraffin Oligomerisation to Aromatics. *Catal. Today* **1990**, *6*, 351–372. [\[CrossRef\]](#)
40. Al-Zahrani, S.M. Catalytic Conversion of LPG to High-Value Aromatics: The Current State of the Art and Future Predictions. *Dev. Chem. Eng. Miner. Process.* **1988**, *6*, 101–120. [\[CrossRef\]](#)
41. Fricke, R.; Kosslick, H.; Lischke, G.; Richter, M. Incorporation of Gallium into Zeolites: Syntheses, Properties and Catalytic Application. *Chem. Rev.* **2000**, *100*, 2303–2405. [\[CrossRef\]](#)
42. Ono, Y.; Kitagawa, H.; Sendoda, Y. Transformation of Lower Alkanes into Aromatic Hydrocarbons over ZSM-5 Zeolites. *J. Jpn. Pet. Inst.* **1987**, *30*, 77–88. [\[CrossRef\]](#)
43. Dooley, K.M.; Chang, C.; Price, G.L. Effects of Pretreatments on State of Gallium and Aromatization Activity of Gallium/ZSM-5 Catalysts. *Appl. Catal. A Gen.* **1992**, *84*, 17–30. [\[CrossRef\]](#)
44. Frash, M.V.; van Santen, R.A. Activation of Small Alkanes in Ga-Exchanged Zeolites: A Quantum Chemical Study of Ethane Dehydrogenation. *J. Phys. Chem. A* **2000**, *104*, 2468–2475. [\[CrossRef\]](#)
45. Meitzner, G.D.; Iglesia, E.; Baumgartner, J.E.; Huang, E.S. The Chemical State of Gallium in Working Alkane Dehydrocyclodimerization Catalysts. In Situ Gallium K-Edge X-ray Absorption Spectroscopy. *J. Catal.* **1993**, *140*, 209–225. [\[CrossRef\]](#)
46. Kazansky, V.B.; Subbotina, I.R.; van Santen, R.A.; Hensen, E.J.M. DRIFTS Study of the Chemical State of Modifying Gallium Ions in Reduced Ga/ZSM-5 Prepared by Impregnation. I. Observation of Gallium Hydrides and Application of CO Adsorption as Molecular Probe for Reduced Gallium Ions. *J. Catal.* **2004**, *227*, 263–269. [\[CrossRef\]](#)

47. Phadke, N.M.; Mansoor, E.; Bondil, M.; Head-Gordon, M.; Bell, A.T. Mechanism and Kinetics of Propane Dehydrogenation and Cracking over Ga/H-MFI Prepared via Vapor-Phase Exchange of H-MFI with GaCl₃. *J. Am. Chem. Soc.* **2019**, *141*, 1614–1627. [\[CrossRef\]](#)
48. Schreiber, M.W.; Plaisance, C.P.; Baumgärtl, M.; Reuter, K.; Jentys, A.; Bermejo-Deval, R.; Lercher, J.A. Lewis-Brønsted Acid Pairs in Ga/H-ZSM-5 to Catalyze Dehydrogenation of Light Alkanes. *J. Am. Chem. Soc.* **2018**, *140*, 4849–4859. [\[CrossRef\]](#) [\[PubMed\]](#)
49. Uslamin, E.A.; Saito, H.; Sekine, Y.; Hensen, E.J.M.; Kosinov, N. Different Mechanisms of Ethane Aromatization over Mo/ZSM-5 and Ga/ZSM-5 Catalysts. *Catal. Today* **2020**, in press. [\[CrossRef\]](#)
50. Ausavasukhi, A.; Sooknoi, T. Tunable Activity of [Ga]HZSM-5 with H₂ Treatment: Ethane Dehydrogenation. *Catal. Commun.* **2014**, *45*, 63–68. [\[CrossRef\]](#)
51. Choudhary, V.R.; Kinage, A.K.; Choudhary, T.V. Low-Temperature Nonoxidative Activation of Methane over H-Galloaluminosilicate (MFI) Zeolite. *Science* **1997**, *275*, 1286–1288. [\[CrossRef\]](#)
52. Solt, H.; Lónyi, F.; Mihályi, R.M.; Valyon, J.; Gutierrez, L.B.; Miro, E.E. A Mechanistic Study of the Solid-State Reactions of H-Mordenite with Indium (0) and Indium (III) Oxide. *J. Phys. Chem. C* **2008**, *112*, 19423–19430. [\[CrossRef\]](#)
53. Price, G.L.; Kanazirev, V.; Dooley, K.M.; Hart, V.I. On the Mechanism of Propane Dehydrocyclization over Cation-Containing, Proton-Poor MFI Zeolite. *J. Catal.* **1998**, *173*, 17–27. [\[CrossRef\]](#)
54. Hart, V.I.; Bryant, M.B.; Butler, L.G.; Wu, X.; Dooley, K.M. Proton-Poor, Gallium- and Indium-Loaded Zeolite Dehydrogenation Catalysts. *Catal. Lett.* **1998**, *53*, 111–118. [\[CrossRef\]](#)
55. Baba, T.; Abe, Y.; Nomoto, K.; Inazu, K.; Echizen, T.; Ishikawa, A.; Murai, K. Catalytic Transformation of Methane over In-Loaded ZSM-5 Zeolite in the Presence of Ethene. *J. Phys. Chem. B* **2005**, *109*, 4263–4268. [\[CrossRef\]](#) [\[PubMed\]](#)
56. Maeno, Z.; Yasumura, S.; Wu, X.; Huang, M.; Liu, C.; Toyao, T.; Shimizu, K. Isolated Indium Hydrides in CHA Zeolites: Speciation and Catalysis for Nonoxidative Dehydrogenation of Ethane. *J. Am. Chem. Soc.* **2020**, *142*, 4820–4832. [\[CrossRef\]](#) [\[PubMed\]](#)
57. Beyer, H.K.; Mihályi, R.M.; Minchev, C.; Neinska, Y.; Kanazirev, V. Study of the Reductive Solid-State Ion Exchange of Indium into an NH₄-Beta Zeolite. *Microporous Mesoporous Mater.* **1996**, *7*, 333–341. [\[CrossRef\]](#)
58. Maeno, Z.; Yasumura, S.; Liu, C.; Toyao, T.; Kon, K.; Nakayama, A.; Hasegawa, J.; Shimizu, K. Experimental and Theoretical Study of Multinuclear Indium-Oxo Clusters in CHA Zeolite for CH₄ Activation at Room Temperature. *Phys. Chem. Chem. Phys.* **2019**, *21*, 13415–13427. [\[CrossRef\]](#)
59. Tsoukalou, A.; Abdala, P.M.; Stoian, D.; Huang, X.; Willinger, M.G.; Fedorov, A.; Müller, C.R. Structural Evolution and Dynamics of an In₂O₃ Catalyst for CO₂ Hydrogenation to Methanol: An Operando XAS-XRD and In Situ TEM Study. *J. Am. Chem. Soc.* **2019**, *141*, 13497–13505. [\[CrossRef\]](#)
60. Zhu, Q.; Kondo, J.N.; Tatsumi, T.; Inagaki, S.; Ohnuma, R.; Kubota, Y.; Shimodaira, Y.; Kobayashi, H.; Domen, K. A Comparative Study of Methanol to Olefin over CHA and MTF Zeolites. *J. Phys. Chem. C* **2007**, *111*, 5409–5415. [\[CrossRef\]](#)
61. Blakeman, P.G.; Burkholder, E.M.; Chen, H.Y.; Collier, J.E.; Fedeyko, J.M.; Jobson, H.; Rajaram, R.R. The Role of Pore Size on the Thermal Stability of Zeolite Supported Cu SCR Catalysts. *Catal. Today* **2014**, *231*, 56–63. [\[CrossRef\]](#)
62. Villamaina, R.; Liu, S.; Nova, I.; Tronconi, E.; Ruggeri, M.P.; Collier, J.; York, A.; Thompson, D. Speciation of Cu Cations in Cu-CHA Catalysts for NH₃-SCR: Effects of SiO₂/Al₂O₃ Ratio and Cu-Loading Investigated by Transient Response Methods. *ACS Catal.* **2019**, *9*, 8916–8927. [\[CrossRef\]](#)
63. Ward, J.W. A Spectroscopic Study of the Surface of Zeolite Y. II. Infrared Spectra of Structural Hydroxyl Groups and Adsorbed Water on Alkali, Alkaline Earth, and Rare Earth Ion-Exchanged Zeolites. *J. Phys. Chem.* **1968**, *72*, 4211–4223. [\[CrossRef\]](#)
64. Duncan, T.M.; Vaughan, R.W. The Adsorption of Formic Acid on Y Zeolites: An Infrared Absorbance Study. *J. Catal.* **1981**, *471*, 469–471. [\[CrossRef\]](#)

